


**Two-dimensional superfluidity in  $^4\text{He}$  clusters intercalated into graphite**Jeonghwan Ahn<sup>1</sup>, Tyler Volkoff<sup>1,2</sup>, Jae-Sung Kim<sup>1,3,4,\*</sup> and Yongkyung Kwon<sup>1,†</sup><sup>1</sup>*Department of Physics, Konkuk University, Seoul 05029, Korea*<sup>2</sup>*Theoretical Division, Los Alamos National Laboratory, Los Alamos, New Mexico 87545, USA*<sup>3</sup>*Department of Physics, Sook-Myung Women's University, Seoul 04310, Korea*<sup>4</sup>*Institute of Advanced Materials and Systems, Sook-Myung Women's University, Seoul 04310, Korea* (Received 29 June 2020; revised 28 September 2020; accepted 12 October 2020; published 30 October 2020)

Motivated by recent technical developments on selective intercalation of inert gases just beneath the surface graphene of graphite, we perform path-integral Monte Carlo calculations to study structural and superfluid properties of  $^4\text{He}$  clusters encapsulated between a bulged surface graphene layer and the graphite (0001) substrate. The intercalated  $^4\text{He}$  atoms initially decorate the inner surface of the bulged graphene to form a shell structure, leaving a void inside it. Then, the additional  $^4\text{He}$  atoms form a disk-shaped liquid platelet in the void, which shows finite superfluid response at temperatures below 1 K. The temperature-dependent superfluid fractions of the platelet follow modified Kosterlitz-Thouless recursion relations, indicating that two-dimensional superfluidity can be realized in an intercalated  $^4\text{He}$  system.

DOI: [10.1103/PhysRevB.102.144527](https://doi.org/10.1103/PhysRevB.102.144527)**I. INTRODUCTION**

Three-dimensional (3D) bulk  $^4\text{He}$  displays a continuous increase in the superfluid density as the temperature decreases. On the other hand, the superfluid transition of a two-dimensional (2D)  $^4\text{He}$  film is characterized by a universal jump of the superfluid density at the critical temperature. In the Kosterlitz-Thouless (KT) theory, this jump is explained by the unbinding mechanism of bound vortex-antivortex pairs [1,2]. The validity of the KT theory for describing 2D  $^4\text{He}$  systems has been borne out by experiments on  $^4\text{He}$  films adsorbed on flat substrates such as a Mylar film [3–6] and subsequently verified by a series of path-integral Monte Carlo (PIMC) calculations of ideal  $^4\text{He}$  films [7–9].

Even finite-sized 3D  $^4\text{He}$  clusters can manifest the superfluid phenomena, which was first predicted in the PIMC study of Sindzingre *et al.* [10] and supported later by a theoretical study based on the quantum-droplet model [11]. Analysis of rotational spectra of impurity molecules embedded into  $^4\text{He}$  nanodroplets provided unequivocal experimental evidence for superfluidity in finite helium systems [12–14]. In contrast, there is presently no comprehensive theoretical and experimental framework to study superfluid properties of geometrically confined, finite 2D  $^4\text{He}$  systems. In this work, we utilize numerical calculations of temperature-dependent superfluid fractions to develop an appropriate modification of the KT theory that allows us to analyze the 2D superfluid transition in an experimentally accessible confined  $^4\text{He}$  system.

The last decade has witnessed the notable development in the controlled intercalation that has proven to be a facile tool to grow the materials in their reduced dimensions such as the 2D platelet and zero-dimensional cluster [15–17]. Espe-

cially, the intercalation of the inert gas selectively between the surface graphene layer and the first subsurface layer of graphite has recently been achieved, by the incidence of low ( $<100\text{ eV}$ ) energy ions on a graphite surface [18], allowing the application of the various surface probes that can investigate the atomic, electronic structures of low-dimensional  $^4\text{He}$  systems and their excitations. Thus intercalated  $^4\text{He}$  systems serve as a test bed for investigation of the superfluid behavior in both reduced dimensions and confined geometries, leading to a deeper understanding of their superfluid origins.

Motivated by these observations, we have performed PIMC calculations for  $^4\text{He}$  systems intercalated beneath the graphite surface to investigate their structural properties and superfluid response. The system is modeled with  $^4\text{He}$  atoms being encapsulated between the domed surface graphene and the adjacent flat graphene as depicted in Fig. 1(a). We find that intercalated  $^4\text{He}$  atoms form a shell structure along with a disk-shaped liquid  $^4\text{He}$  platelet inside the shell. The superfluid fractions of the  $^4\text{He}$  platelet computed as a function of temperature are well fitted to modified KT recursion relations, signifying the 2D nature of its superfluidity. Furthermore, the estimated vortex core energies and diameters are comparable to the corresponding values reported for an extended 2D  $^4\text{He}$  film [7]. To our best knowledge, this is the first theoretical prediction of the 2D superfluidity in a finite system.

**II. METHODOLOGY**

For this study, we assume that only the surface graphene layer is deformed by the  $^4\text{He}$  intercalation to form the truncated hemisphere. The height of the truncated hemisphere and the radius of its projection onto the basal plane are set to be 10 and 20 Å, respectively. This bulged graphene layer exhibits a shape similar to the graphene nanobubbles formed by  $^4\text{He}$  atoms trapped between surface graphene and mica substrate [19].

\*jskim@sm.ac.kr

†ykwon@konkuk.ac.kr

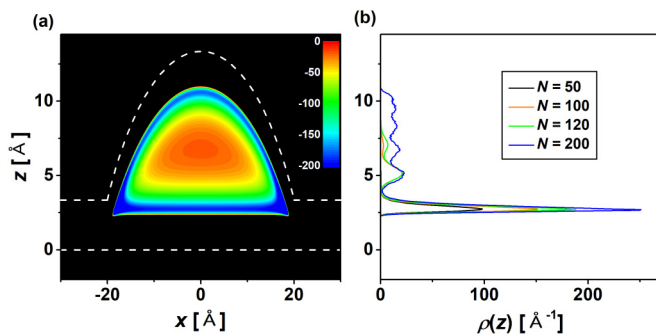


FIG. 1. (a) A contour plot of the potential energy  $V(x, z)$  between deformed graphite layers and an encapsulated  ${}^4\text{He}$  atom. Here the  $z$  axis is perpendicular to the graphite surface and goes through the dome center of the deformed graphene (the upper dotted line).  $z = 0$  is set to be the vertical position of the second topmost graphene (the horizontal dotted line). The contour plot is presented in the color scale denoted by the color bar in units of kelvins. (b) One-dimensional density distribution  $\rho(z)$  of  $N$   ${}^4\text{He}$  atoms encapsulated within the graphite layers.

The interaction between a  ${}^4\text{He}$  atom and each graphene layer is described in terms of a laterally averaged one-dimensional (1D)  ${}^4\text{He}$ -graphene potential  $V_{1D}(l_{\min})$  proposed by Carlos and Cole [20,21] where  $l_{\min}$  is the shortest distance between  ${}^4\text{He}$  and graphene. The resulting  ${}^4\text{He}$ -substrate potential energy is displayed in Fig. 1(a). For the  ${}^4\text{He}$  -  ${}^4\text{He}$  interaction, a well-known Aziz potential [22] is employed. Because the exact form of thermal many-body density matrix is not known at a low temperature  $T$ , it is described by a convolution of  $M$  high-temperature density matrices with an imaginary time step  $\tau = (Mk_B T)^{-1}$  in the discrete path-integral representation [23,24]. We use pair product forms of the exact two-body density matrices [23] derived at the high temperature  $MT$ , which are found to provide accurate descriptions for both  ${}^4\text{He}$  -  ${}^4\text{He}$  and  ${}^4\text{He}$ -substrate interactions with a time step  $\tau^{-1}/k_B = 40$  K. The accuracy of these density matrices was also confirmed in the previous PIMC studies for  ${}^4\text{He}$  atoms adsorbed on graphene [25] and graphite surfaces [26]. The simulations are performed under free boundary conditions in all directions and the simulation cell size is set to be  $40 \times 40 \times 20 \text{ \AA}^3$ .

### III. RESULTS

Figure 1(b) presents one-dimensional density profiles  $\rho(z)$  as a function of the vertical distance  $z$  from the second topmost graphene layer for different numbers of the intercalated  ${}^4\text{He}$  atoms  $N$ . One can observe a sharp peak located at  $z \sim 2.7 \text{ \AA}$  and, at larger distances, a spread in the  ${}^4\text{He}$  density where the peaks are not distinctly separated. The sharp peak indicates the formation of a 2D structure at the bottom, which results from the interaction between  ${}^4\text{He}$  atoms and the second topmost graphene at  $z = 0 \text{ \AA}$ . Note that this bottom 2D  ${}^4\text{He}$  structure is separated from the underlying flat graphene by  $\sim 2.7 \text{ \AA}$ , the same as the distance between the first adsorbed  ${}^4\text{He}$  layer and the graphite surface [26,27]. The vertical separation is also consistent with the previous result of molecular

dynamics simulations for the layered structure of helium bubble trapped between a surface graphene and mica substrate [19]. For  $N = 50$ ,  $\rho(z)$  vanishes beyond the sharp peak, indicating that the bottom 2D structure is developed first. As more  ${}^4\text{He}$  atoms are intercalated, the additional helium atoms are expected to form a capping layer beneath the truncated hemisphere of the surface graphene.

To see the intercalated structures of  ${}^4\text{He}$  atoms in more detail, we present the density distribution projected onto the  $r$ - $z$  plane  $\rho(r, z)$ , where  $r$  represents the distance from the  $z$  axis, for  $N = 240$  in Fig. 2(a). The horizontally aligned density peaks at  $z \sim 2.7 \text{ \AA}$  represent  ${}^4\text{He}$  atoms constituting the basal plane that corresponds to the sharp peak observed in Fig. 1(b). The capping layer is developed along the truncated hemisphere of the surface graphene, which, combined with the  ${}^4\text{He}$  basal plane, forms a shell structure. A similar shell structure was also predicted to form inside a spherical cavity [28].

The 2D density distribution  $\rho(x, y)$  of  ${}^4\text{He}$  atoms in the basal plane for  $N = 240$  is displayed in Fig. 2(b) where well-defined peak positions are arranged with the triangular order, indicating their solidification. The average  ${}^4\text{He}$  -  ${}^4\text{He}$  distance in the basal plane is estimated to be  $\sim 3.1 \text{ \AA}$ , which is comparable to the range  $3.1$ - $3.17 \text{ \AA}$  reported for the completed first  ${}^4\text{He}$  layer on a flat graphite surface [27,29–32]. This suggests that the adsorption of  ${}^4\text{He}$  atoms in the basal plane is mainly controlled by their interaction with the underlying flat graphene layers but affected little by the overlying bulged graphene.

The development of  ${}^4\text{He}$  structures inside the shell is now investigated with the increasing number of  ${}^4\text{He}$  atoms. The bottom panel of Fig. 2 presents 2D density distributions  $\rho(x, y)$  of inner  ${}^4\text{He}$  atoms on top of the basal  ${}^4\text{He}$  plane for  $N = 240, 270$ , and  $300$ , where surrounding shell structures show little difference from each other, nearly identical to the one presented in Figs. 2(a) and 2(b). From Fig. 2(c), along with Fig. 2(a), one can see that  ${}^4\text{He}$  atoms settled inside the shell form a quasi-2D helium liquid as evidenced by the disk-shaped, delocalized density distribution. On the other hand, distinct density peaks are observed in Fig. 2(d), signaling solidification of some inner  ${}^4\text{He}$  atoms for  $N = 270$ . The  ${}^4\text{He}$  atoms inside the shell eventually form a triangularly ordered structure for  $N = 300$  as displayed in Fig. 2(e). One expects that physical properties of these inner  ${}^4\text{He}$  platelets are distinct from those of  ${}^4\text{He}$  atoms in the shell because the platelet  ${}^4\text{He}$  structures mainly result from the  ${}^4\text{He}$  -  ${}^4\text{He}$  interaction, not from the  ${}^4\text{He}$ -graphite interaction.

In the Feynman path-integral formalism on which the PIMC method is based, exchange-coupled Feynman paths that are comparable to the system size signify superfluidity of a Bose liquid. In the linear response regime, an estimator of the superfluid fraction involves the projected area of the Feynman paths [23],

$$f_\alpha^s = \frac{4m^2 \langle A_\alpha^2 \rangle k_B T}{\hbar^2 I_\alpha^{cl}}, \quad (1)$$

where  $A_\alpha$  is the area of a Feynman path projected onto a plane perpendicular to the principal axis  $\hat{x}_\alpha$  and  $I_\alpha^{cl}$  is a diagonal

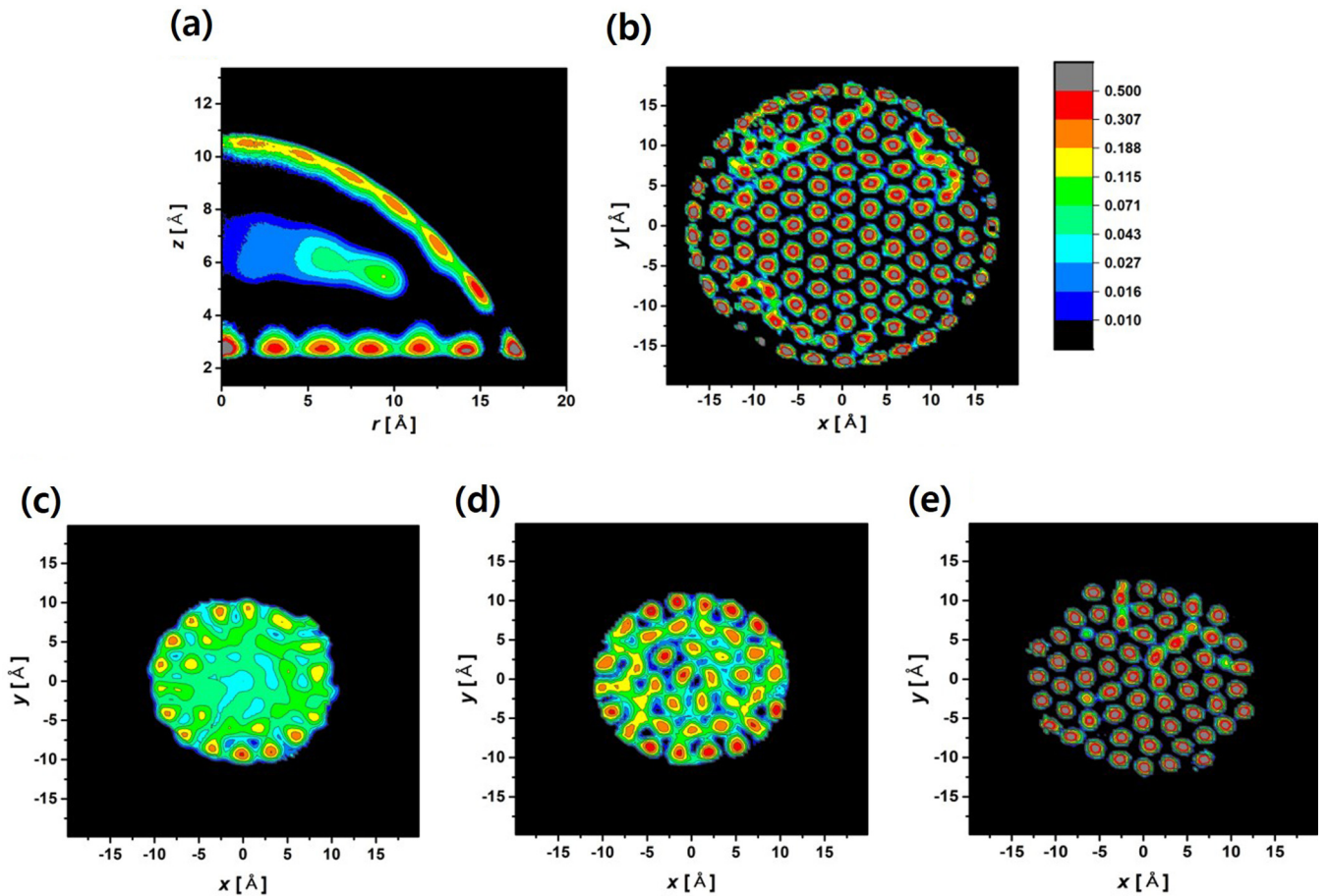


FIG. 2. (a) Two-dimensional  ${}^4\text{He}$  density distribution  $\rho(r, z)$  for  $N = 240$  and (b) its bottom-layer density distribution  $\rho(x, y)$ , along with two-dimensional density distributions  $\rho(x, y)$  of the inner  ${}^4\text{He}$  platelets for (c)  $N = 240$ , (d)  $N = 270$ , and (e)  $N = 300$ . The computations were performed at a temperature of 0.5 K and the length scale is  $\text{\AA}$ . The contour plots are presented in the same color scale denoted by the color bar (log scales) in the upper right hand corner.

element of the classical moment of inertia tensor. Since it was first employed by Sindzingre *et al.* [10] for pure clusters of a few tens of  ${}^4\text{He}$  atoms, this area estimator and its local decompositions [33,34] have been successfully applied to investigate the superfluid responses of various finite  ${}^4\text{He}$  systems. We also investigate the superfluidity of the  ${}^4\text{He}$  platelet confined inside the shell using the superfluid estimator of Eq. (1). For this, the exchange samplings are implemented only among  ${}^4\text{He}$  atoms inside the shell, which is justified by the fact that  ${}^4\text{He}$  atoms in the shell are strongly bound to the adjacent graphene surface and their contributions to exchange path samplings are negligible.

Figure 3(a) shows the superfluid fraction  $f^s$  of the platelet at a temperature 0.5 K, with respect to the number  $N_{\text{inner}}$  of  ${}^4\text{He}$  atoms in the platelet. For  $N_{\text{inner}} = 20$ , the superfluid fraction is negligible, indicating that the platelet is too dilute to be in a superfluid state. For  $30 \leq N_{\text{inner}} \leq 60$ , however, the platelet shows substantial superfluid response  $f_z^s$  to the rotation around the axis ( $z$  axis) perpendicular to the graphite surface while the superfluid response  $f_{x,y}^s$  to the rotation about the lateral ( $x$  or  $y$ ) directions is significantly suppressed. This anisotropic superfluid response is consistent with the above observation that the  ${}^4\text{He}$  atoms inside the shell form a disk-

shaped platelet. Negligible superfluid fractions for  $N_{\text{inner}} > 60$  are attributed to the solidification of  ${}^4\text{He}$  atoms in the platelet, which can be seen in Fig. 2. The trend of decreasing superfluid fraction as the solidification proceeds is also observed in 2D  ${}^4\text{He}$  films [8] and  ${}^4\text{He}$  layers adsorbed inside a spherical glass cavity [28].

Figure 3(b) shows the temperature dependence of  $f_z^s$  for different values of  $N_{\text{inner}}$ . We observe the onset of the superfluid state below 1 K and the saturation of  $f_z^s$  to values less than unity in the limit of  $T$  going to 0 K. The saturated superfluid fractions can be attributed to the confined geometries of the  ${}^4\text{He}$  platelets as well as their finite sizes. Note that the enhanced surface effects in a 2D platelet compared to a 3D cluster can result in the observed reduction of low-temperature superfluid fraction; the  ${}^4\text{He}$  atoms in the surface region are less involved in exchange-coupled paths than the atoms in the interior, while the fraction of the surface atoms is larger in a 2D platelet than in a 3D cluster. We also find that the saturated value of  $f_z^s$  decreases with increasing  $N_{\text{inner}}$ , which can be understood by the solidification of  ${}^4\text{He}$  atoms in the platelet.

Noting that our  ${}^4\text{He}$  platelet inside the shell can be considered as a fragment of an extended 2D film, we analyzed the



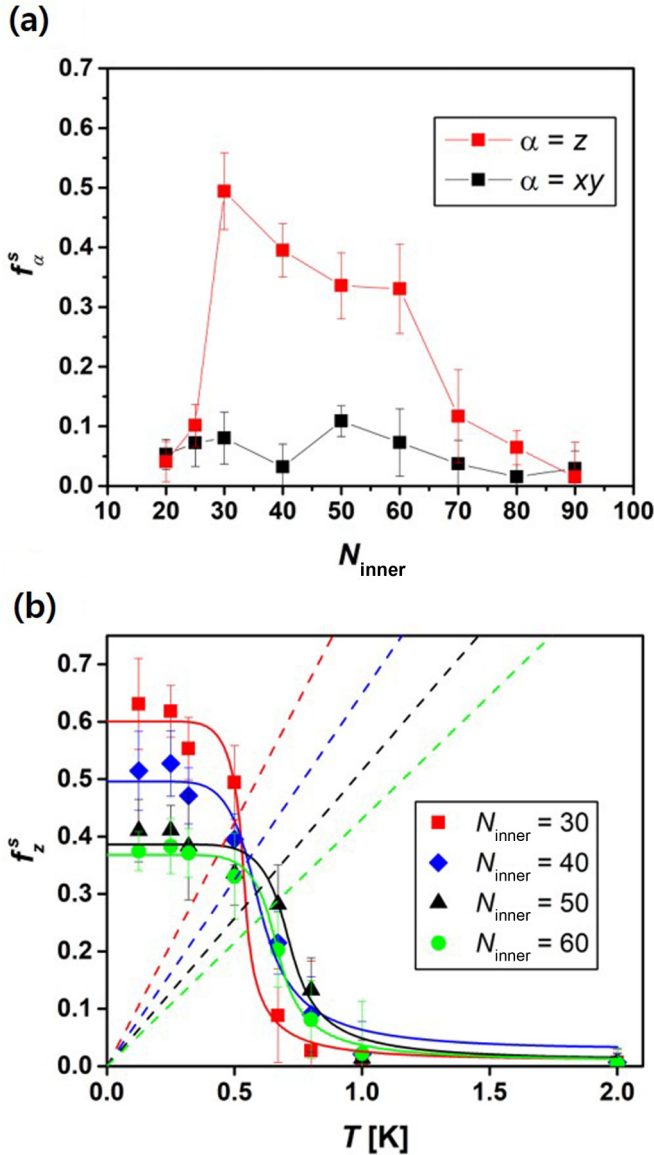


FIG. 3. (a) Superfluid fraction as a function of the number of the inner  $^4\text{He}$  atoms  $N_{\text{inner}}$  at a temperature of 0.5 K along the vertical ( $z$ ) and the lateral ( $x, y$ ) directions. (b) Superfluid fraction along the  $z$  axis as a function of temperature for different numbers of the inner  $^4\text{He}$  atoms. The solid lines represent the fitting lines with the modified KT recursion relations of Eq. (2) while the dotted lines denote the universal-jump relation predicted in the KT theory.

temperature dependence of  $f_z^s$  through the KT recursion relations that were previously used for finite-size analysis of the superfluid  $^4\text{He}$  film [7,9]. In order to reconcile the observed low-temperature superfluid fraction with the traditional KT theory, we transform the original KT recursion equations into integral equations for  $f_z^s$  and further introduce the physical parameter  $\sigma$  that corresponds to the zero-temperature ( $\beta \rightarrow \infty$ ) saturation value of  $f_z^s(\beta; l)$ :

$$f_z^s(\beta; l) = \frac{1}{\frac{1}{\sigma} + 8\lambda\rho\beta\pi^3 \int_0^l dl' y(\beta; l')^2},$$

$$y(\beta; l) = y(\beta; 0) e^{\int_0^l dl' [2 - 2\pi\beta\lambda\rho f_z^s(\beta; l')]}, \quad (2)$$

TABLE I. Fitting parameters estimated with the modified KT recursion relations. Here,  $E_c$  and  $d$  represent the vortex core energy and diameter, respectively, while  $\sigma$  corresponds to the saturated superfluid fraction.

$N_{\text{inner}}$ :	30	40	50	60
$E_c$ (K)	1.66(6)	1.79(5)	1.29(7)	1.34(6)
$d$ (Å)	7.15(8)	7.19(6)	8.55(8)	6.90(8)
$\sigma$	0.61(4)	0.50(4)	0.39(3)	0.37(3)

where  $y(\beta; 0) = e^{-\beta E_c}$ ,  $l = \ln \frac{L}{2d}$ , and  $\lambda = \frac{\hbar^2}{2m}$ . [Note that the fugacity  $y(\beta; l)$  exponentially approaches zero as  $T \rightarrow 0$  K]. Values of  $\sigma < 1$  indicate a departure from the well-known superfluid transition of an extended 2D  $^4\text{He}$  film [7,9]. The fitting parameters  $E_c$  and  $d$  correspond to the vortex core energy and the core diameter, respectively, while the system length scale  $L$  is set to be 25 Å, the diameter of our disk-shaped  $^4\text{He}$  platelet. The best-fit parameters  $E_c$ ,  $d$ , and  $\sigma$  are summarized in Table I. The estimated values of  $E_c$  and  $d$  for our system are consistent with the corresponding values predicted for the extended  $^4\text{He}$  film [7,9], indicating a similar vortex unbinding mechanism of the superfluid transition in these systems. More specifically, while our estimated values of  $E_c$  are comparable to  $2.18 \pm 0.04$  K [9] and  $2.7 \pm 0.2$  K [7] predicted for the  $^4\text{He}$  film, our vortex diameters are close to  $8.8 \pm 0.5$  Å reported in Ref. [9], rather than  $3.7 \pm 0.4$  Å of Ref. [7], for the  $^4\text{He}$  film.

The solid lines in Fig. 3(b) indicate that the least-squares fits of the computed  $f_z^s$  to the KT recursion relations consistently describe the temperature dependence of the superfluid behaviors for all  $N_{\text{inner}}$ . This confirms the 2D nature of superfluidity of our  $^4\text{He}$  platelet encapsulated by graphite layers. Based on the KT theory for the 2D superfluidity, we now estimate the critical temperatures for the superfluid transitions of our  $^4\text{He}$  platelets. The dashed lines in Fig. 3(b) represent the universal jump relations of  $f_s(T_c^-) = \frac{2mk_B T_c}{\hbar^2 \pi \rho}$ , whose intersections with the fitted curves determine the critical temperatures of the superfluid transitions. Note that the same procedure was used to determine the critical temperature of a  $^4\text{He}$  film from the PIMC superfluid fraction data which also exhibited the smeared-out transition due to the finite sizes of the simulation cells [7–9], similar to our PIMC data shown in Fig. 3(b). The estimated critical temperatures are found to be in the range of 0.51 K ( $N_{\text{inner}} = 30$ )  $\sim$  0.62 K ( $N_{\text{inner}} = 60$ ), which is slightly lower than the transition temperatures of 0.65 to 0.90 K predicted for extended  $^4\text{He}$  films [7–9]. This discrepancy results from the suppressed low-temperature superfluidity due to the finite size of our  $^4\text{He}$  platelet, which makes its superfluidity more vulnerable to thermal fluctuation than that of the extended 2D system.

Despite the discoidal shape of the  $^4\text{He}$  platelet inside the shell, its density distribution shows a sizable spread along the vertical direction compared to that at the basal plane as shown in Fig. 2(a). Thus, it is remarkable that superfluidity of the  $^4\text{He}$  platelet is well described by a simple modification to the KT theory for the 2D superfluid transition, indicating that the vertical atomic motions contribute little to the vortex nucleation, binding, and unbinding. According to the torsional oscillator experiments of Nyeki *et al.* [35] as well as Crowell

and Reppy [36,37], the superfluid transition in the second  ${}^4\text{He}$  layer on graphite is not characterized by the KT theory. On the other hand, the superfluid response of the third  ${}^4\text{He}$  layer on graphite was described by a broadened KT transition, analogous to superfluid properties of our  ${}^4\text{He}$  platelets. The  ${}^4\text{He}$  platelet neighbors both the  ${}^4\text{He}$  capping layer and the  ${}^4\text{He}$  basal plane. The presence of the capping layer weakens effective coupling of the  ${}^4\text{He}$  platelet to the underlying basal plane. This might be a reason why the superfluid behavior of our  ${}^4\text{He}$  platelet is similar to that of the third  ${}^4\text{He}$  layer on graphite, rather than the second  ${}^4\text{He}$  layer.

#### IV. CONCLUSION

We have investigated the structural properties and superfluid response of  ${}^4\text{He}$  platelets intercalated beneath the graphite surface. Our PIMC calculations indicate that  ${}^4\text{He}$  intercalation proceeds with the formation of the shell structure composed of adsorbed  ${}^4\text{He}$  atoms, which is followed by the growth of a finite-size 2D  ${}^4\text{He}$  liquid platelet inside the shell. Furthermore, the superfluid state of the  ${}^4\text{He}$  platelets at moderate densities below 1 K is well described by a low-temperature modification of the KT theory, indicative of 2D

superfluidity in a finite system. Our proposed system consisting of  ${}^4\text{He}$  atoms intercalated beneath the graphite surface allows the application of various surface probes and opens the possibility of exploring 2D nanoscale superfluidity at tunable helium densities by manipulation of the intercalated atoms. We therefore expect this system to serve as a facile test bed for analysis of superfluidity of a finite 2D  ${}^4\text{He}$  platelet.

#### ACKNOWLEDGMENTS

Y.K. was supported by the Basic Science Research Program (2018R1D1A1B07042443) through the National Research Foundation of Korea funded by the Ministry of Education. J.-S.K. was supported by the National Research Foundation of Korea through Grants No. NRF-2016R1D1A1B03930532 and No. NRF-2019R1F1A1040955. T.J.V. acknowledges support from the Laboratory Directed Research and Development program at Los Alamos National Laboratory. We also acknowledge the support from the Supercomputing Center/Korea Institute of Science and Technology Information with supercomputing resources including technical support (KSC-2019-CRE-0200).

- 
- [1] J. M. Kosterlitz and D. J. Thouless, *J. Phys. C: Solid State Phys.* **6**, 1181 (1973).
- [2] J. Kosterlitz, *J. Phys. C: Solid State Phys.* **7**, 1046 (1974).
- [3] D. J. Bishop and J. D. Reppy, *Phys. Rev. Lett.* **40**, 1727 (1978).
- [4] D. J. Bishop and J. D. Reppy, *Phys. Rev. B* **22**, 5171 (1980).
- [5] D. McQueeney, G. Agnolet, and J. D. Reppy, *Phys. Rev. Lett.* **52**, 1325 (1984).
- [6] G. Agnolet, D. F. McQueeney, and J. D. Reppy, *Phys. Rev. B* **39**, 8934 (1989).
- [7] D. M. Ceperley and E. L. Pollock, *Phys. Rev. B* **39**, 2084 (1989).
- [8] M. C. Gordillo and D. M. Ceperley, *Phys. Rev. B* **58**, 6447 (1998).
- [9] M. Boninsegni, N. V. Prokof'ev, and B. V. Svistunov, *Phys. Rev. E* **74**, 036701 (2006).
- [10] P. Sindzingre, M. L. Klein, and D. M. Ceperley, *Phys. Rev. Lett.* **63**, 1601 (1989).
- [11] K. B. Whaley, *Intern. Rev. Phys. Chem.* **13**, 41 (1994).
- [12] M. Hartmann, F. Mielke, J. P. Toennies, A. F. Vilesov, and G. Benedek, *Phys. Rev. Lett.* **76**, 4560 (1996).
- [13] S. Grebenev, J. P. Toennies, and A. F. Vilesov, *Science* **279**, 2083 (1998).
- [14] J. P. Toennies, A. F. Vilesov, and K. B. Whaley, *Phys. Today* **54**, 31 (2001).
- [15] M. Petrović, I. Š. Rakić, S. Runte, C. Busse, J. Sadowski, P. Lazić, I. Pletikosić, Z.-H. Pan, M. Milun, P. Pervan *et al.*, *Nat. Commun.* **4**, 2772 (2013).
- [16] Y. S. Park, J. H. Park, H. N. Hwang, T. S. Laishram, K. S. Kim, M. H. Kang, and C. C. Hwang, *Phys. Rev. X* **4**, 031016 (2014).
- [17] Q. Fu and X. Bao, *Chem. Soc. Rev.* **46**, 1842 (2017).
- [18] S. Yoo, E. Åhlgren, J. Seo, W. Kim, S. Chiang, and J. Kim, *Nanotechnology* **29**, 385601 (2018).
- [19] H. Ghorbanfekr-Kalashami, K. Vasu, R. Nair, F. M. Peeters, and M. Neek-Amal, *Nat. Commun.* **8**, 15844 (2017).
- [20] W. E. Carlos and M. W. Cole, *Surf. Sci.* **91**, 339 (1980).
- [21] M. W. Cole and J. R. Klein, *Surf. Sci.* **124**, 547 (1983).
- [22] R. A. Aziz, M. J. Slaman, A. Koide, A. R. Allnatt, and W. J. Meath, *Mol. Phys.* **77**, 321 (1992).
- [23] D. M. Ceperley, *Rev. Mod. Phys.* **67**, 279 (1995).
- [24] R. E. Zillich, F. Paesani, Y. Kwon, and K. B. Whaley, *J. Chem. Phys.* **123**, 114301 (2005).
- [25] Y. Kwon and D. M. Ceperley, *Phys. Rev. B* **85**, 224501 (2012).
- [26] J. Ahn, H. Lee, and Y. Kwon, *Phys. Rev. B* **93**, 064511 (2016).
- [27] P. Corboz, M. Boninsegni, L. Pollet, and M. Troyer, *Phys. Rev. B* **78**, 245414 (2008).
- [28] M. Boninsegni, *Phys. Rev. B* **92**, 174112 (2015).
- [29] M. Bretz, J. Dash, D. Hickernell, E. McLean, and O. Vilches, *Phys. Rev. A* **8**, 1589 (1973).
- [30] P. A. Whitlock, G. V. Chester, and B. Krishnamachari, *Phys. Rev. B* **58**, 8704 (1998).
- [31] S. Nakamura, K. Matsui, T. Matsui, and H. Fukuyama, *J. Low Temp. Phys.* **171**, 711 (2013).
- [32] S. Nakamura, K. Matsui, T. Matsui, and H. Fukuyama, *Phys. Rev. B* **94**, 180501(R) (2016).
- [33] E. W. Draeger and D. M. Ceperley, *Phys. Rev. Lett.* **90**, 065301 (2003).
- [34] Y. Kwon, F. Paesani, and K. B. Whaley, *Phys. Rev. B* **74**, 174522 (2006).
- [35] J. Nyéki, A. Phillis, A. Ho, D. Lee, P. Coleman, J. Parpia, B. Cowan, and J. Saunders, *Nat. Phys.* **13**, 455 (2017).
- [36] P. A. Crowell and J. D. Reppy, *Phys. Rev. Lett.* **70**, 3291 (1993).
- [37] P. A. Crowell and J. D. Reppy, *Phys. Rev. B* **53**, 2701 (1996).